Counterintuitive multiphoton pulse sequences in molecular isomerization. I. Selectivity and robustness of competing multiphoton stimulated Raman adiabatic passage processes

Imrich Vrábel[a] and Werner Jakubetz[b]
Institut für Theoretische Chemie und Molekulare Strukturbiologie, Universität Wien, Währinger Str. 17, A-1090 Wien, Austria

(Received 9 September 2002; accepted 24 December 2002)

We use a 28-level system consisting of the vibrational bend states of the HCN/HNC system as a model system for the investigation of population transfer across the isomerization barrier using counterintuitively ordered multiphoton (MP) laser pulses. This $(m+n)$-STIRAP (stimulated Raman-adiabatic passage) arrangement with m pump- and n Stokes-photons is found to be capable of driving HCN→HNC transition states selectively and in a robust manner, despite the presence of near-degenerate parallel processes of different photonicities. Employing Gaussian pulses with widths of 80 ps, the process of highest photonicity we demonstrate is (4+6)-STIRAP, and we investigate systematically the robustness against variations in pulse amplitudes and frequencies for all parallel processes with $m=2$ and 3, and $n=1-6$. We discuss the conditions under which selective population transfer is obtained. We also compare with (1+1)-STIRAP using overtone transitions to drive the same state-specific processes and conclude that the few-step sequential MP-STIRAP isomerization is a feasible alternative to the sequential (1+1)-STIRAP based method proposed by Kurkal and Rice [J. Phys. Chem. B **105**, 6488 (2001)]. © *2003 American Institute of Physics.* [DOI: 10.1063/1.1545773]

I. INTRODUCTION

Isomerization, hydrogen transfer, and other unimolecular reactions proceeding on the electronic ground state potential surface may be induced and driven by infrared laser pulses, with the prospect of active laser control.[1] In the most simplistic model,[2] such reactions are represented by two localized states, the reactant state, and the product state, separated by a barrier and connected by a delocalized state in the barrier region, i.e., a transition state. In the language of quantum optics this case is represented by a three-level system (TLS) in Λ-configuration, and thus potentially the arsenal of methods developed for population transfer in TLSs (Ref. 3) is applicable to the control of unimolecular reactions.

In particular, pump–dump (PD) strategies[1–3] involving two resonant π-pulses,[4] which transfer the system first to the delocalized apex state of the Λ and then on to the product state, closely mimic collisional chemistry with its reaction through the transition state: they are (chemically) ''intuitive.'' However, stringent conditions with respect to resonance frequencies and pulse areas must be met in order to achieve efficient population transfer.[3,4] Considering velocity and orientational distributions of the target particles and natural temporal and spatial variations in the laser pulses, the lack of robustness with respect to the pulse parameters can lead to difficulties in the experimental implementation of such π-pulse methods. Robust mechanisms are also important for the success of laboratory methods generating laser fields by self-learning feedback techniques.[5–7]

Chemically less intuitive strategies may be invoked to obtain robust methods for reaction control. Population transfer by stimulated Raman adiabatic passage (STIRAP) (Refs. 3, 8–12) is a particularly robust scheme. In this technique a ''counterintuitive'' sequence of pulses is employed, in which the dump-laser, in this context generally referred to as Stokes-laser, precedes the pump laser. If population transfer proceeds adiabatically, the intermediate level remains unpopulated, and a transfer efficiency of 100% may be achieved over an extended region of pulse parameter space. In an application to a model chemical reaction, the STIRAP scheme was used by Ohta *et al.*[13] to control the intramolecular hydrogen transfer in a three-level asymmetric double-well potential. They show that in such a model complete ''isomerization,'' i.e., population transfer from one local minimum state to the other, is possible using a counterintuitive pulse sequence.

Obviously models using TLSs can only demonstrate the principles of laser control of chemical reactions, but cannot quantitatively reproduce the processes occurring in real systems. Realistic reactive systems are multi- (N-)level systems (NLSs) with an extended Λ-structure. In order to describe *state specific* isomerization, the initial and final states of the TLS are each replaced by a specific level out of large sets of vibrational or vibrotational reagent and product levels, and similarly a set of delocalized levels above the barrier may have to replace the single apex level. Furthermore, intricate coupling relations including various overtone- and through-barrier couplings as well as couplings to background states

[a]Deceased. Imrich Vrábel died in a car accident, age 31, while conducting the research reported here. This paper is dedicated to his memory.
[b]Author to whom correspondence should be addressed. Electronic mail: werner.jakubetz@univie.ac.at

will modify the structure of these systems, turning them into fairly complex networks dominated by a Λ-like backbone.

In order to implement PD and STIRAP techniques in such situations, generalizations of these techniques to NLSs are required. In principle, a generalization of the PD scheme is straightforward and may involve series of sequential pump and dump pulses or multiphoton (MP) pump and dump pulses in place of single-photon ones, or even sequences of such MP pulses. The former scenario has been pioneered in particular by Manz and co-workers,[2,14] who have simulated laser induced isomerization and proton transfer in one dimensional (1D) N-level model systems by series of simple IR pulses. During the pump stage, the molecule is intermediately prepared in different excited vibrational states in the reactant well *en route* from the initial reactant state up to a delocalized state. Similarly, during the dump stage the molecule is prepared in different product states *en route* from the delocalized state down to a final target product state. Sequences of MP pump and dump pulses have also been used to drive the prototype isomerization HCN→HNC state-specifically using a three-dimensional (3D) Hamiltonian.[15]

The extension of the STIRAP to more complex cases has two aspects. The first one is the introduction of additional levels into the basic TLS. Coulston and Bergmann[10] have worked out the conditions under which STIRAP transfer remains efficient if additional levels in various configurations are coupled to the TLS. The second aspect, the introduction of multistep cases, may be based on concepts similar to those used in PD strategies. Thus Kurkal and Rice[16] recently proposed the use of a *sequence* of simple consecutive STIRAP steps. Utilizing stretch-overtone transitions, they simulated HCN→HNC isomerization from ground state to ground state proceeding on a time scale of nanoseconds. Alternatively, several multipulse extensions of the STIRAP scheme have been proposed for population transfer in extended NLSs. In one of these methods the total ordering of all individual subpulses is counterintuitive.[17,18] Alternatively, the counterintuitive pulse ordering is only partially maintained; all even-numbered pulses in the sequence precede all the pulses corresponding to odd transitions.[19] This latter scheme, denoted ''alternating STIRAP,'' is restricted to sequentially coupled systems with an odd number of levels. Finally a third scheme denoted ''straddling STIRAP'' was proposed for arbitrary sequentially coupled NLSs and involves a counterintuitive sequence of partially overlapping Stokes and pump pulses, straddled by pulses on resonance with all intermediate transitions.[20] All these methods use $N-1$ overlapping pulses for N levels, which may make the experimental realization less attractive in molecular systems with a high density of vibrational states.

Interesting possibilities exist for extending conventional STIRAP to situations in which the pump and Stokes interactions involve MP transitions.[18,21–23] In this case, the usual (1+1)-STIRAP scheme (one pump photon and one Stokes photon) is modified to a MP-STIRAP, more precisely to an $(m+n)$-STIRAP scheme (m pump photons and n Stokes photons). The suitability of this technique for the infrared excitation of vibrational levels had been pointed out in Ref. 18, but few explicit theoretical studies of MP STIRAP in realistic molecular systems seem to have been carried out.[22,24] For small photonicities m and n a number of general properties of such processes in model few-level systems have been derived,[21,22] usually invoking effective MP Hamiltonians. Thus in the ideal limit the existence of an adiabatically evolving two-color Floquet state[25] connecting initial state and target state (a ''connected state'') is an important requirement for the success of the method. Typically this transfer state will acquire contributions from intermediate states, the latter hence no longer being true spectator states. It has also been shown that in contrast to simple STIRAP, corrections to the rotating wave approximation (RWA) are substantial in MP-STIRAP and may alter the qualitative picture of the process.[21]

The application of MP-STIRAP to more extended realistic molecular systems poses several challenges. In particular, long anharmonic progressions may be expected to limit the frequency ranges accessible to individual $(m+n)$ processes. Irregularities and degeneracies in the anharmonic progressions will arise both from the more complex shapes of three-dimensional potentials and from the interaction between the reactant and product ladder states. Very high-lying states may passively participate via the dynamical Stark shifts they induce. Coupling to a fairly dense manifold of background states may perturb the STIRAP transitions. Furthermore, the focus of MP-STIRAP should be on driving transitions with fairly high photonicities—or otherwise the method would not provide a competitive alternative to (1+1)-STIRAP strategies.

Another interesting point is the total process duration. The adiabaticity criterion[8–12,26] in effect requires the pulse area, conveniently expressed in multiples of π, to be large, and the pulse shape to change slowly. For NLSs and MP-processes the literal pulse area must be replaced by a generalized pulse area (GPA),[27,28] and the two may differ greatly in numerical value. Irrespective of such subtleties this comes down to the condition that the individual pulses should be long. Yet short pulses may be desirable in many situations. Thus self-learning adaptive pulse-shaping, which would benefit from robust mechanisms, for practical reasons is limited to the lower picosecond range.[6,7] The question then is if and how far away the MP-STIRAP can be pushed from the adiabatic limit, towards shorter pulses,[26] and how this would affect its robustness.

In a series of papers we explore these points on the basis of simulations for model NLSs with realistic molecular parameters based on three-dimensional (3D) wave functions. In the present part I we show the feasibility of MP population transfer across a barrier by counterintuitively ordered pulses in extended Λ-NLSs. In particular, we demonstrate $(m+n)$-STIRAP, $m=2-4$, $n=1-6$, across the barrier of the HCN→HNC isomerization reaction, proceeding along the manifolds of the HCN- and HNC-bend vibrations. In the adiabatic limit, which in view of the many possible antagonistic perturbations in the present system we place at GPAs around and in excess of 100π, the corresponding pulse widths are about 50 ps and longer; as our standard example we use pulsewidths of 80 ps. The important question of ro-

bustness is addressed by mapping out the frequency and amplitude ranges leading to near-complete state-specific isomerization, and the performance of MP-STIRAP is compared to that of (1+1)-STIRAP. These results are discussed in view of the complications associated with near-degeneracies and overlapping resonances along the anharmonic progressions, and we attempt to relate the results to analytical solutions concerning the robustness[8–12,26] of standard STIRAP in a TLS.

In follow-up papers[29] we will provide a detailed analysis of the properties, mechanisms and population dynamics of individual $(m+n)$-STIRAP processes, also in conjunction with the use of this technique with much shorter pulses. We will also address additional complications stemming from phase-sensitive behavior associated both with a possible fortuitous commensurability of the pump- and Stokes-frequencies and with the coupling to background states in systems with a higher density of vibrational states. Such complications may prevent the free choice of the photonicities and may restrict the applicability of $(m+n)$-STIRAP to selected combinations of m and n.

The rest of the present paper is organized as follows: In Sec. II we describe the computational models and techniques used in our simulations. Section III will be devoted to an analysis of the specific properties of the extended Λ-system formed by the vibrational bend states of the HCN/HNC system. In Sec. IV we present the results for $(2+n)$- and $(3+n)$-STIRAP processes across the HCN→HNC isomerization barrier over extended ranges of pulse amplitudes, frequencies and durations, and discuss the issue of robustness. We also give a brief account of (4+6)-STIRAP, which is the transition of highest overall photonicity we have treated. Finally, a summary and our conclusions are in Sec. V.

II. COMPUTATIONAL DETAILS

We consider the interaction of a nonrotating oriented molecule in its electronic ground state, specified by the molecular Hamiltonian $\hat{H}_0$ and the dipole moment operator $\boldsymbol{\mu}$, with a laser pulse. The excitation of vibrational modes by a laser field is described within the semiclassical dipole approximation. The molecule interacting with the laser field is represented by the time-dependent Hamiltonian,

$$\hat{H}=\hat{H}_0-\boldsymbol{\mu}\cdot\mathbf{E}(t). \tag{1}$$

The laser pulse is specified by the field strength vector $\mathbf{E}(t)$. We assume the field to be linearly polarized in a plane parallel to the molecular axis. In our simulations for the HCN/HNC system this axis is the C–N bond, fixed along the x-axis of a space-fixed coordinate system. Using $\mathcal{E}(t)=|\mathbf{E}(t)|$, the interaction term in Eq. (1) takes the form $\mu_x\mathcal{E}(t)$.

A. Pulses

The pulse setup and the most important pulse characteristics are schematically depicted in Fig. 1. Throughout the investigations presented in this paper we use simple Gaussian pulse pairs. As noted above, all pulses are assumed to be polarized in a plane parallel to the CN axis, and the overall field $\mathcal{E}(t)$ is then given by

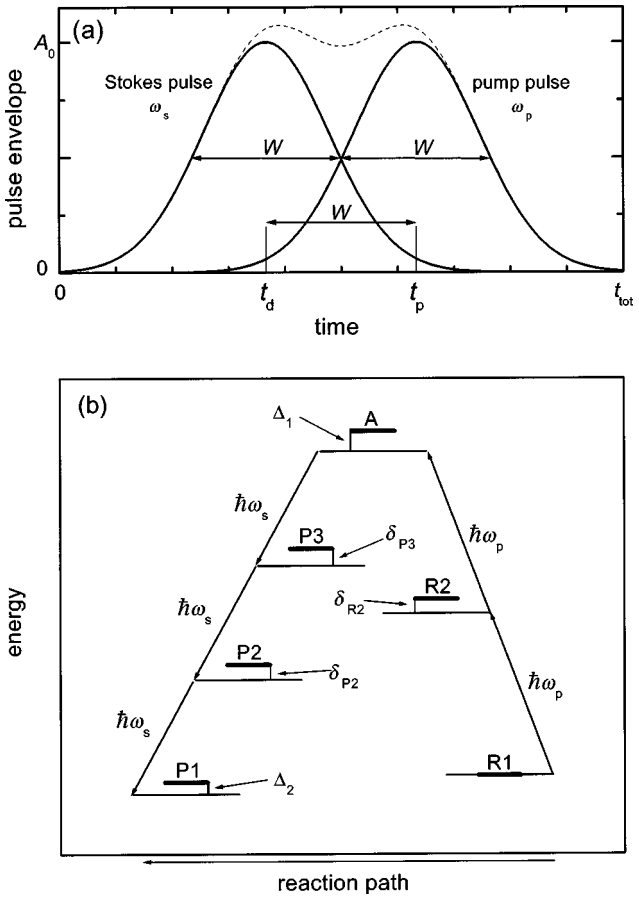

FIG. 1. Schematic representation of the counterintuitively ordered pulse pair and the MP-STIRAP process across the barrier in an extended Λ-system. (a) The pulse configuration used throughout this paper. The pump- (p-) and Stokes- (s-)pulses have equal Gaussian envelope functions with peak amplitude A_0 and width W; the Stokes pulse precedes the pump pulse by the time delay -W. (b) A (2+3) STIRAP process leading from the initial reagent (R) state $R1$ to the target product (P) state $P1$ via the intermediate reagent state $R2$, the apex state A and the intermediate product states $P3$ and $P2$. For pump frequency ω_p and Stokes frequency ω_s the figure shows the intermediate-level detuning Δ_1, the overall detuning Δ_2, and the rung detunings δ_i for $i=R2$, $P2$, and $P3$.

$$\mathcal{E}(t)=f(t,t_p)A_{0,p}\sin(\omega_p t+\varphi_p) + f(t,t_s)A_{0,s}\sin(\omega_s t+\varphi_s). \tag{2}$$

The subscripts p and s denote, respectively, the individual pump- and Stokes-pulses with central frequencies ω_p and ω_s, initial phases φ_p and φ_s, and peak amplitudes $A_{0,p}$ and $A_{0,s}$. The Gaussian envelope function

$$f(t,t_k)=\exp\{-(t-t_k)^2/2\gamma_k^2\}, \tag{3}$$

with k standing for either p or s, specifies a pulse centered at time t_k, with width parameter γ_k corresponding to a pulse width $W_k=(8\ln 2)^{1/2}\gamma_k$ (full width at half height).

In order to mimic laboratory conditions that are as simple as possible, we constrain the pump- and Stokes-pulses to have equal envelopes, i.e., in each $(m+n)$-STIRAP pulse pair, both pulses have equal widths, $W_p=W_s=W$, and

equal amplitudes, $A_{0,p}=A_{0,s}=A_0$. The pulse delay $\Delta t=t_p-t_s$ is kept fixed at $\Delta t=-W$, resulting in counterintuitive ordering. This configuration is the one shown in Fig. 1(a). It has been analyzed for (1+1)-STIRAP in a TLS, and it has been shown that the particular pulse delay chosen above is an optimal choice in a certain sense.[9,11] However, in the present NLS these pulses, which have equal literal pulse areas, are not matched with respect to their GPAs, and the weaker of the two transitions will determine the degree of adiabaticity of the total setup. Although the above constraints give rise to a considerable reduction of the available parameter space, they do not severely limit the possibility to devise pulse pairs yielding complete or near-complete population transfer. This behavior indicates the relative robustness of the STIRAP transfer mechanism.

At "initial time" $t_i=t_s-1.875W_s$ and "final time" $t_f=t_p+1.875W_p$ the amplitude functions have numerically died out for all practical purposes, so that the field is effectively "off" outside the interval $[t_i, t_f]$. This means that in our specific setup a MP-STIRAP process with individual pulsewidths W can be assigned a total duration $t_{\mathrm{tot}}=t_f-t_i=3.75W$. For $W=80$ ps as used in the examples in Sec. IV, this corresponds to $t_{\mathrm{tot}}=300$ ps. Without loss of generality the time scale is chosen such that $t_i=0$, and the phase φ_s in Eq. (2) is set to zero. We also use $\varphi_s=0$ throughout, since the investigation of phase-sensitive behavior is beyond the scope of this paper. The results discussed here are indeed not or only very weakly phase-dependent—although phase-sensitive behavior does appear for commensurate values of ω_p and ω_s.[28] In Sec. IV A we will briefly return to this point.

Figure 1(b) illustrates the energy and frequency relations for a pulse pair acting on states in an extended Λ-configuration. Here and in the following we will identify "reagent" states (HCN states in the HCN→HNC isomerization) by the label Ri, where i represents a number in a suitable numbering scheme, "product" (HNC) states analogously by Pi, and the apex state of the extended Λ-system by A (we will later have to deal with multiple apex states, which we will number as Ai). The figure indicates various detunings playing important roles in the MP-STIRAP processes associated with pump frequency ω_p and Stokes frequency ω_s; the intermediate-level detuning Δ_1 (the detuning of the pump pulse from its MP zero-order resonance), the overall detuning Δ_2 [the detuning from the $(m+n)$-photon zero-order resonance], and the rung detunings δ_i measuring the mismatch between intermediate rungs of the anharmonic ladder of molecular levels and the harmonic MP ladder. In case ω_p and ω_s are chosen to equal the zero-order resonance frequencies $\omega_{0,p}$ and $\omega_{0,s}$ we have $\Delta_1=\Delta_2=0$, and the rung level detunings δ_i assume the values $\delta_{0,i}$.

B. Molecular Hamiltonian, vibrational energy levels, and dipole matrix

As in previous model investigations of HCN→HNC isomerization[15,30] we use 3D vibrational wave functions[31] and dipole moment functions[15] derived from *ab initio* calculations, from which we also determine the dipole matrix elements $\mu_{ij}=\langle i|\mu_x|j\rangle$.

Sets of $J=0$ and $J=1$ vibrational eigenstates of $\hat{H}_0$ have been obtained by Bowman *et al.*[31] The states below the isomerization barrier are strongly (>98%) localized in either the HCN or the HNC well of the potential energy surface (PES). These states $|i\rangle$, with eigenvalues ε_i, can be characterized by triples of quantum numbers (v_1,v_2,v_3) corresponding to the normal modes of the isomers, i.e., C–H or N–H stretch, H–C–N or H–N–C bend, and C–N stretch. Higher levels above the barrier may still be localized on one of the two isomers, but delocalized states with various degrees of delocalization become increasingly important with increasing energy.

Pure bend states of HCN and HNC, with quantum numbers $(0,v_2,0)$, are spread out along the minimum energy path for isomerization on both sides of the barrier, and extend also into the energy regime above the barrier. They provide the most efficient sequentially coupled ladders for reaching and crossing the barrier[15] and are a natural choice for MP strategies of isomerization. In particular, in a rotation-free model of isomerization the $J=K=0$ states $(0,v_2,0)$, which have v_2 even, give rise to an extended Λ-NLS suitable for MP-STIRAP transfer by pulses polarized along the CN axis.

The energy level diagram of the 28 lowest states of this type (cumulative for both isomers) is shown in Fig. 2. We use v_2 to number the levels of this 28-level system (28-LS), labeling the HCN (reagent) states by Rv_2 and the HNC (product) states by Pv_2, hence $R0$ to $R26$ and $P0$ to $P26$ for the levels included. However, $R24$ and $P24$ exist only as zero-order states. As will be discussed in Sec. III, they interact to form a pair of completely delocalized states at the apex of the extended Λ-system formed by the two bend progressions. In energetic ordering, these two otherwise equivalent apex states are denoted $A1$ and $A2$.

This 28-LS forms the basis set employed to obtain the results presented in Sec. IV. It contains all the states which are absolutely essential to describe the MP-dynamics for pulses in the frequency range of the bend transitions, being either directly involved in the transitions or contributing noticeably through their dynamical Stark shifts. It neglects weakly coupled or far off-resonant states (background states) and high-lying states well above the barrier. The influence of these neglected states is explored elsewhere.[29]

C. Time-dependent Schrödinger equation and pulse optimization

Using the ingredients introduced in Secs. II A and II B, the time-dependent Schrödinger equation describing the evolution of the time-dependent system wave function $|\Psi\rangle$ under the action of the laser field can be integrated. The computational techniques have been presented in Ref. 32. In the energy representation, $|\Psi\rangle$ is expanded in a finite basis set of bound eigenstates $|i\rangle$ of $\hat{H}_0$,

$$|\Psi\rangle=\sum_{i=1}^{N} c_i(t)|i\rangle. \tag{4}$$

The Schrödinger equation can then be written in algebraic form as

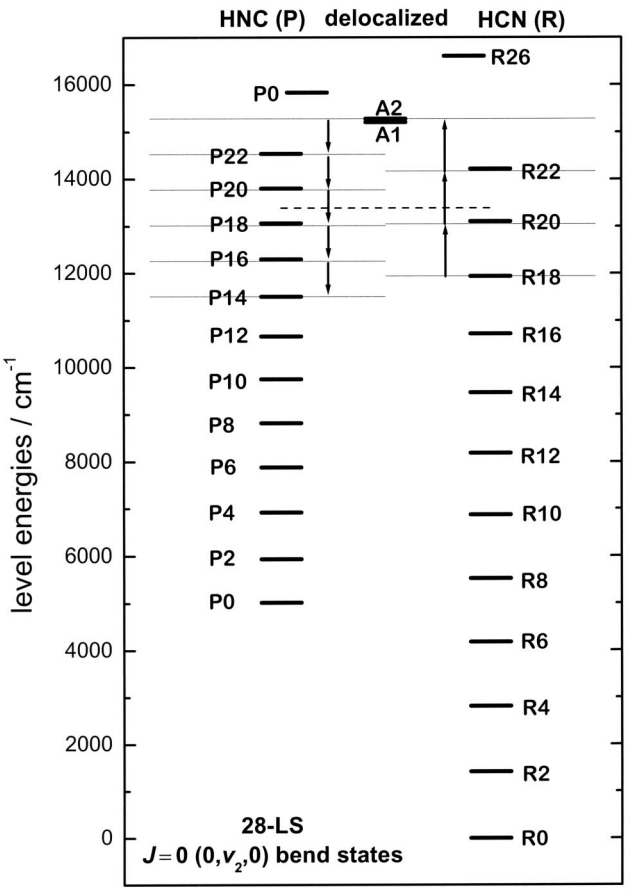

FIG. 2. Level diagram of the 28-LS formed by the $J=0$ vibrational bend eigenstates $(0,v_2,0)$ of the HCN/HNC system. The states are labeled as reactant (HCN) states Rv_2 or product (HNC) states v_2 except for the two delocalized combination states $A1$ and $A2$ at the apex of the extended Λ-system, which are formed from the zero order states HCN(0,24,0) and HNC(0,24,0). The bare classical barrier height at 16 389 cm^{-1} is indicated by a dashed line. The equally spaced thin lines connected by arrows show the zero-order energetics of the (3+5)-STIRAP process leading from the initial state $R18$, HCN (0,18,0), to the target state $P14$, HNC (0,14,0), via the apex state $A2$.

$$i\hbar\dot{\mathbf{c}}=\mathbf{H}\mathbf{c}, \tag{5}$$

where $\mathbf{c}$ is the vector of expansion coefficients $c_i(t)$, and the matrix elements of the Hamiltonian matrix $\mathbf{H}$ are

$$H_{ij}=\varepsilon_i\delta_{ij}-\mu_{ij}A(t). \tag{6}$$

We do not invoke RWA, since it has been shown that this approximation may fail to correctly describe important dynamical features of MP-STIRAP.[21]

Assuming the system to be initially in one of the reagent eigenstates $|Rv_2\rangle$, the set of coupled differential equations (5) is propagated from $t=0$ to $t=t_{\mathrm{tot}}$ using Runge–Kutta or predictor–corrector techniques. Because of the nonstiff nature of the equations it is no problem to converge these integrations even though they run over many thousands of optical cycles. In our examples we assume that the initial state is one of the states $R16$, $R18$, or $R20$, which connect to the apex state ($A1$ or $A2$), respectively, by a 4-, 3-, or 2-photon pump transition. We do not consider the preparation of the excited initial state, but we note that in a complete sequential MP-STIRAP isomerization scenario *a la* Kurkal and Rice,[16] it would have been reached from the ground state in predecessor-MP-STIRAP steps.

The objective of state-specific isomerization is to arrive, at times $t>t_{\mathrm{tot}}$, at a state $|\Psi\rangle$ localized at the product isomer, which is as close as possible to a specified target eigenstate $|Pv_2\rangle$. Our examples address $(m+1)$ to $(m+6)$ STIRAP processes, so that the target states are the HNC levels from $R22$ successively down to $R12$.

We have successfully optimized MP-STIRAP pulse pairs[33] using constrained optimal control algorithms.[1,34,35] However, the rich structure of the probability landscape, with multiple local maxima and flat and extended plateaus, may lead to a strong dependence of the predicted ''optimum'' both on the initial conditions and on details of the algorithm. Furthermore, since in the present investigation we are strongly interested in characterizing the robustness of the method, we require information on the dynamics across extended ranges of parameter space. To this end we obtain results on multidimensional grids of pulse parameters and study the corresponding topographical maps.

III. PROPERTIES OF THE EXTENDED Λ-SYSTEM OF BEND STATES

In order to interpret the dynamics of the transitions and to appreciate some notable differences to simple model systems it is useful to discuss the main features of the 28-LS shown in Fig. 2, which also forms the basis set for our calculations. The lowest 12 $J=0$ bend states of each isomer, i.e., the states (0,0,0) to (0,22,0), labeled, respectively, $R0$ to $R22$ and $P0$ to $P22$, which are below the vibrationally adiabatic barrier (although the uppermost of them are above the *bare* potential barrier), are strongly localized in their respective potential wells. These states form two anharmonic progressions determined by the properties of the two potential wells, with different fundamental frequencies (1419 cm^{-1} for HCN versus 920 cm^{-1} for HNC), and different anharmonic distortions. Due to a shoulder in the HNC well of the PES,[31] the states $R16$ to $R22$ show irregularities in their spacings.

Both bend progressions extend into the range above the barrier, where they interact more strongly with other states. The two highest states shown, $R26$ and $P26$, have dominant leading contributions from bend states, but they do also have some admixtures of other zero-order states. They are weakly delocalized, and they are both distinctly detuned from a regular anharmonic ladder.

The most important feature in the above-barrier range is the strong interaction between the pair of near-degenerate zero-order bend states (0,24,0) of HCN and HNC. The zero-order states combine to form a pair of completely delocalized states denoted $A1$ and $A2$ with an energy gap of 71 cm^{-1}. These combination states have similar coupling elements to the neighboring levels on both sides of the bend ladders and both of them are thus part of both bend progressions. They form a doubled or split apex of the extended Λ-configuration modeling isomerization and represent the transition state of the HCN→HNC isomerization.

The energetic properties of the 28-LS shown in Fig. 2 have important consequences for the population transfer in

TABLE I. Zero-order frequencies and maximum ladder rung detunings for some pump and Stokes transitions involving the delocalized states $A1$ or $A2$ as apex (A) states.

		$A=A1$		$A=A2$	
Transition	Type	ω_0[a]	$\delta_{\max}$[b]	ω_0[a]	$\delta_{\max}$[b]
$R18\rightarrow A$	3-photon pump	1112.61	56.12	1088.80	102.04
$A\rightarrow P22$	1-photon Stokes	741.14	⋯	669.72	⋯
$A\rightarrow P20$	2-photon Stokes	737.17	3.97	701.45	31.73
$A\rightarrow P18$	3-photon Stokes	737.04	4.10	713.23	43.51
$A\rightarrow P16$	4-photon Stokes	743.62	19.74	725.76	56.04
$A\rightarrow P14$	5-photon Stokes	754.40	52.08	740.11	80.64
$A\rightarrow P12$	6-photon Stokes	769.41	103.16	757.51	132.84

[a]Zero-order resonance frequency in cm^{-1}.
[b]Maximum ladder rung detuning in cm^{-1}.

this system. First, because both delocalized states may act as the apex of the Λ-configuration, isomerization may involve competing and parallel interfering pathways. Second, due to the resulting energy shifts in $A1$ and $A2$ relative to the zero-order bend states, additional irregularities are introduced into the anharmonic progressions, which lead to remarkably close near-degeneracies in the transition frequencies for transitions of different photonicities. Third, the irregular spacings also give rise to sizable rung detunings in the individual MP transitions to and from the apex states.

These points are illustrated by the zero-order frequencies ω_0 and the maximum ladder rung detunings $\delta_{\max}$ for the $(3+n)$-STIRAP processes, which are collected in Table I. For an individual MP pump or Stokes transition, $\delta_{\max}$ is defined as $\delta_{\max}=\max\{|\delta_{0,i}|,\ i=\text{all intermediate rungs}\}$. Because of the smaller values of $\delta_{\max}$ for all listed ladders, $A2$ is expected to be the preferred intermediate state for the MP-STIRAP processes. On the other hand, no near-degeneracies occur in the Stokes transitions from state $A1$, whereas we notice pronounced near-degeneracies in the zero-order frequencies for the 1- through 4-PTs from $A2$ to HNC bend states. Indeed, the near-degeneracy between the 2- and 3-PTs is so close, that the frequency distribution of any pulse shorter than about 100 ps will tend to couple these transitions. The splittings between the 1-photon- and each of the 2-, 3-, and 4-photon Stokes transitions are somewhat larger, but this still means that pulses with widths in the lower ps range may fail to be state-selective. Competing parallel processes and the formation of superposition states must be expected to occur in any isomerization strategy involving ps pulses in $(m+1)$- to $(m+4)$-processes, which might affect the feasibility or at least the robustness of MP-STIRAP.

In effect the 28-LS represents an extended and distorted version of the 4- and 5-LSs investigated by Coulston and Bergmann.[10] In particular, the doubling of the apex state and the extension of the ladders above the apex are explicitly considered in Ref. 10, and conditions for the maintenance of efficient adiabatic transfer are derived. Our results will illustrate whether these conditions are met for MP-STIRAP transfer in a system with realistic molecular parameters, far beyond the realm of analytical analysis. Yet it should be remembered that notwithstanding its realistic traits and its *ab initio* background, due to the approximations included in the construction of the Hamiltonian our 28-LS is a *model* system applicable for feasibility studies in a general qualitative sense; it cannot be predictive in terms of direct experimental verification.

IV. MP-STIRAP POPULATION TRANSFER ACROSS THE HCN→HNC ISOMERIZATION BARRIER

In this section we give an overview of the $(m+n)$-STIRAP processes across the HCN→HNC isomerization barrier, with $m=2$ and 3 and $n=1-6$. We investigate the feasibility of state-selective population transfer and the robustness of the method in a system characterized by the presence of several near-degenerate and competing transitions. As a brief summary it can be stated beforehand that state-specific MP-STIRAP population transfer across the isomerization barrier can be readily achieved, and despite the pronounced near-degeneracies in the Stokes frequencies for $n=1-4$, *all* the individual transitions up to $n=6$ can be driven selectively. Our main objective now is to characterize the robustness of the method with respect to variations in the essential pulse characteristics: the intensity (field strength) and the pump and Stokes frequencies.

For this investigation we have adjusted the pulse width such that under the constraint of equal pump- and Stokes-pulse envelopes and with ''typical'' values of the amplitude as discussed below, the system is well in the adiabatic domain, so that a substantial degree of robustness is also guaranteed. For the present system, this is achieved by ascertaining that the corresponding GPAs approach or exceed 100π. As already noted above, this condition is met if the pulse width is chosen as $W=80$ ps. For STIRAP in simple TLS, without considering issues of robustness GPAs as small as $3-4\pi$ would suffice for adiabatic behavior.[11]

Data for selected STIRAP pulse pairs that transfer population via the apex state $A2$ are collected in Table II. Under the same conditions pulses involving transitions through $A1$, which are generally less efficient, have areas that are about 30% smaller. Note the GPAs do not scale linearly with the literal areas under the envelopes or with A_0 (sometimes not even approximately).

A. Frequency variation

State-selective population transfer in $(m+n)$-STIRAP can be accomplished over remarkably extended ranges of

TABLE II. Generalized pulse areas for selected resonant multiple-π-pulses.[a]

Transition	States	A_0 /a.u.	Generalized area/π
2-photon pump	$R18 \rightarrow A2$	0.0017	157
3-photon pump	$R16 \rightarrow A2$	0.00255	111
2-photon Stokes[b]	$A2 \rightarrow P20$[b]	0.0017	217
		0.00255	292
3-photon Stokes[b]	$A2 \rightarrow P18$[b]	0.0017	234
		0.00255	323
4-photon Stokes	$A2 \rightarrow P16$	0.0017	173
		0.00255	260
5-photon Stokes	$A2 \rightarrow P14$	0.0017	86
		0.00255	168
6-photon Stokes	$A2 \rightarrow P12$	0.0017	20
		0.00255	76
1-photon first overtone pump	$R18 \rightarrow A2$	0.0017	42
		0.012	300
1-photon second overtone pump	$R16 \rightarrow A2$	0.00255	8
		0.012	40
1-photon third overtone Stokes	$A2 \rightarrow P16$	0.0017	7
		0.012	54
1-photon fourth overtone Stokes	$A2 \rightarrow P14$	0.00255	3
		0.012	18

[a]Determined from the number of Rabi cycles and rounded to integers.
[b]Prepares a superposition state.

pump- and Stokes-frequencies. In order to provide a comprehensive picture of the set of processes belonging to a fixed pump-photonicity m, it is necessary to map out $\omega_p - \omega_s$ ranges of about $100 \times 200\ \mathrm{cm}^{-1}$. This means that only a coarse frequency grid can be used to obtain representations of the probability landscapes. Figures 3 and 4 show such coarse-grained product-state resolved intensity plots with a frequency resolution of $5\ \mathrm{cm}^{-1}$. The different target states are identified by the number of Stokes photons (n), and shaded areas identify frequency combinations giving rise to near-complete state specific population transfer (shaded cells denote population transfer exceeding 75%). In addition nonshaded, but labeled cells indicate population transfer of 50%–75%.

Before commenting on the results it should be pointed out that the final populations are not strictly phase-independent. Weak sensitivity of the results on the phases φ_p and φ_s may arise whenever a pulse pair prepares a superposition state. In general such phase effects give rise to variations of $<5\%$ in the level populations. Hence they do not lead to any notable changes in the intensity maps and can safely be neglected. However, from this discussion we must exclude a stripe of frequency combinations along the dashed line tagged 3:2, where the pump- and Stokes-frequencies are commensurate with ratio 3:2. In this stripe the MP-STIRAP results can display massive phase sensitivity. This situation will be considered elsewhere.[29] The results included, for completeness, in the present figures are those for the arbitrary special case $\varphi_p = \varphi_s = 0$. This is also the choice made for the remaining range, where, as said, the results do not significantly depend on the specific values of the phases.

Figure 3 shows results for $(2+n)$-STIRAP processes for two values of the pulse amplitude, $A_0 = 0.0017$ a.u., corresponding to a laser peak intensity of about $100\ \mathrm{GW\,cm}^{-2}$, and $A_0 = 0.0030$ a.u., corresponding to about $300\ \mathrm{GW\,cm}^{-2}$. For the various individual transitions, these values translate into the GPAs given in Table II. The results for the lower of the two field strengths are shown in Fig. 3(a). Here the most dominant feature is the extended contiguous frequency range in which near-complete $(2+1)$-transfer is achieved. However, in view of our objective to bridge as many quanta as possible, the results for $n>1$ are of greater interest. Indeed there are sizable ranges of robustness for the $(2+2)$-, $(2+3)$-, and $(2+4)$-transitions, and even $(2+5)$-STIRAP proceeds in a fairly robust manner.

The qualitative aspects of successful state-specific MP-STIRAP transfer can be related to the web of lines superimposed on the intensity plot, which represent various zero-detuning situations. The two vertical lines indicate the zero-order frequencies for the 2-photon pump transitions to $A1$ (at $1048\ \mathrm{cm}^{-1}$) and to $A2$ (at $1085\ \mathrm{cm}^{-1}$) and hence zero intermediate-level detuning; along these lines we have $\Delta_1 = 0$. The full lines denote zero overall detuning for the $(2+n)$-processes indicated. The condition $\Delta_2 = 0$ is independent of the apex state, and for the $(m+n)$-process is met along a straight line with slope n/m.

Pump frequencies below $\approx 1060\ \mathrm{cm}^{-1}$ have Δ_1 considerably larger for the transition through the apex state $A2$ than for transition through $A1$, and we may expect that population transfer will mainly involve the latter state. The corresponding zero order Stokes frequencies are well separated (cf. Table I), and so it is not surprising that the zones of near-complete population transfer are also well separated and can form sizable contiguous regions of robustness. As anticipated from the rung level detunings of the various MP transitions in Table I, this mechanism is more efficient for $n=1$ and 2 than for the transitions of higher photonicity. Although some $(2+3)$- and $(2+4)$-population transfer through $A1$ does occur at the lower field strength, these transitions predominantly proceed through $A2$, as does $(2+5)$-STIRAP. But in the range where transfer through $A2$ is expected to be preferable, i.e., for $\omega_p > 1065\ \mathrm{cm}^{-1}$, the degeneracies among the various $(2+n)$-transitions are pronounced, the individual processes of different photonicity compete and do no longer occur in well-separated frequency domains. While state-specific transfer to any of the product states under consideration occurs readily, the frequency ranges supporting any of those transitions disintegrate into several disjoint parts, interspersed with ranges of stability of different transitions. As a whole, these individual ranges form a compact, but intricate pattern that appears to be difficult to predict or analyze.

Nevertheless it can be stated that these individual ranges sow a propensity for approximate zero overall detuning. This is not meant to imply that tuning both pulses on (zero-order) resonance is the optimum strategy for MP-STIRAP. In fact the maxima (centers of plateaus and ridges) of the two-color $(m+n)$-photon resonance are detuned from their zero-order values (which is expected in view of the dynamical Stark shifts). However, the extent of the observed shift differs widely for the various transitions and individual zones of stability. The overall detuning may reach amazing values; red shifts of $60\ \mathrm{cm}^{-1}$ and more are observed for the $(2+1)$-transition, difficult to explain by dynamical Stark shifts alone.

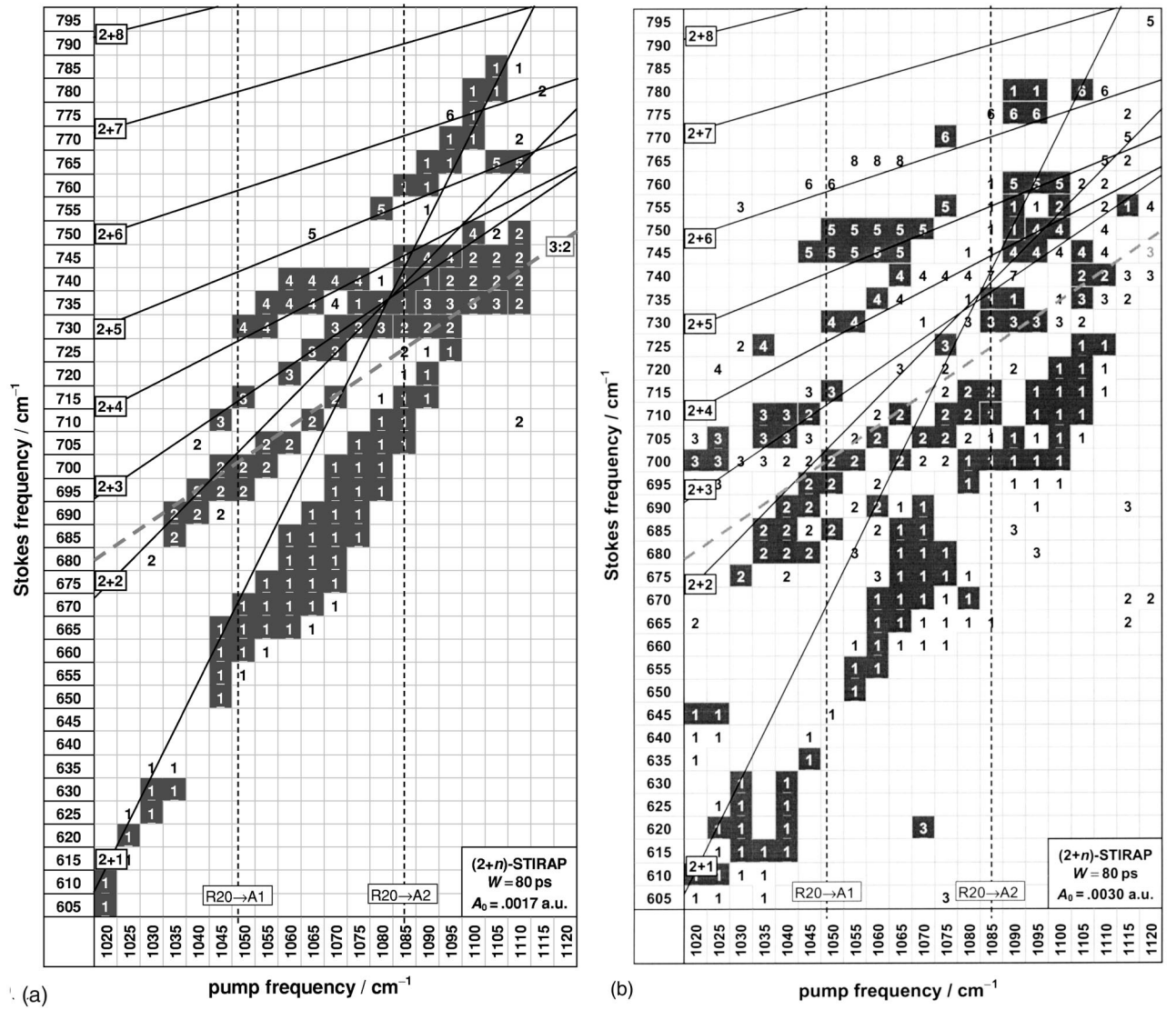

FIG. 3. Coarse-grained final-state resolved intensity plot for $(2+n)$-STIRAP processes. The frequency resolution is 5 cm^{-1}. All pulses have $W=80$ ps. (a) $A_0=0.0017$ a.u.; (b) $A_0=0.0030$ a.u. (these values of A_0 correspond to GPAs given in Table II). A number n in a cell denotes a dominant $(2+n)$ population transfer with >50% final population of the target state. Shaded cells indicate near-complete population transfer, with >75% final population in the target state. Full lines superimposed on the plot represent the zero-overall detuning condition $\Delta_2=0$ for the transition indicated by the tag. Vertical broken lines denote the zero intermediate-level detuning condition $\Delta_1=0$ for transitions through the apex state $A1$ or $A2$ as indicated by the tag. The gray broken line tagged "3:2" represents the commensurability condition $2\omega_p=3\omega_s$.

In fact two contributions to these displacements can be discerned. The small shift observed notably for the transitions not strongly affected by degeneracy problems, e.g., for $(2+5)$ and $(2+6)$, which is reminiscent of the resonance defects and Bloch–Siegert shifts of one-color π-pulse resonances,[36] is linked to the dynamical Stark shifts. On the other hand, the very strong detuning for $(2+1)$-STIRAP must be seen as an *apparent* shift related to the competition with near-degenerate parallel processes of different photonicity. For blueshifted frequencies the competing higher-order transitions affect and quench the $(2+1)$-process, while if *both* frequencies are redshifted, only the $(2+1)$ transition can proceed, since then all other transitions are far too strongly detuned. It is this asymmetric quenching that pushes the center of the stability range far towards the red. We will readdress this point in Sec. III B.

While the overall detuning can be sizable in some regions, the pattern of the intensity plot as a whole is still governed by the zero-overall detuning conditions. Individual zones of robustness tend to be extended in the direction along or parallel to their zero-overall detuning lines, indicating liberal variation of the intermediate-level detuning and much less variability of the overall detuning.

At the higher field strength, illustrated in Fig. 3(b), the relative importance of the transitions with higher photonicities is increased. The contribution of the $(2+1)$-process is becoming less prominent, while the importance of the MP Stokes transitions of higher photonicity is considerably amplified, and extended ranges of robustness appear for the $(2+5)$- and $(2+6)$-transitions. This behavior can be related to the fact that increasing the field strength has two antagonistic effects. On the one hand, the GPAs are increased, thus in

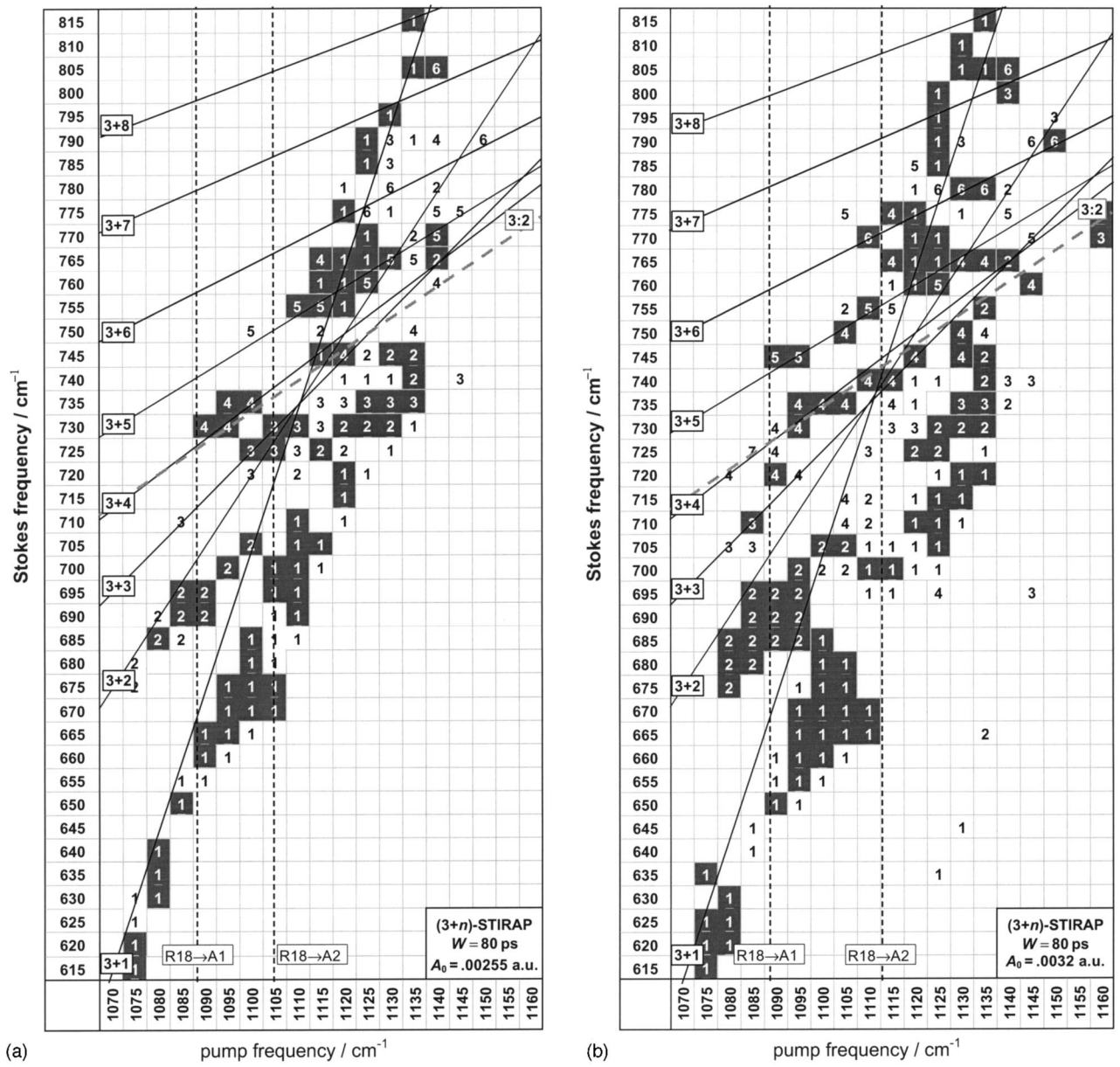

FIG. 4. Coarse-grained final-state resolved intensity plot for $(3+n)$-STIRAP processes. (a) $A_0=0.00255$ a.u.; (b) $A_0=0.0032$ a.u. All other details are as in Fig. 3.

principle shifting the conditions further towards the adiabatic limit. This effect becomes most strongly apparent for the weakest MP-transitions, i.e., the processes with high Stokes-photonicities, in particular if proceeding through $A1$. The larger GPAs also admit increased intermediate-level detuning.[12] This gives rise to the appearance of regions of efficient state-specific population transfer in the peripheral parts of the frequency range mapped out in Fig. 3.

Conversely stronger fields also produce increased coupling between individual transitions and enhances the formation of superposition states in regions that lead to state-selectivity for the lower field. This coupling is most strongly felt in the area around the closely spaced zero-order transition frequencies for the processes through $A2$. For the lower field, for which Stokes coupling is still weak, a fairly compact "tiling" of the $\omega_p-\omega_s$ plane with regions of state-specific population transfer is apparent in Fig. 3(a). This compact zone appears thinned out in Fig. 3(b). Overall, the intensity plot at higher field strength appears more extended, but less compact than the one at lower field strength.

From Fig. 4 it is seen that the $(3+n)$-STIRAP processes show the same qualitative behavior as their $(2+n)$-counterparts, although the individual zones of stability are smaller. Due to the higher pump photonicity, higher field strengths are required to obtain sufficiently large GPAs. The intensity plots in Figs. 4(a) and 4(b) have been obtained for $A_0=0.00255$ and 0.0032 a.u. At these field strengths, the high-photonicity transitions $(3+5)$- and $(3+6)$-STIRAP proceed without problems.

In additional runs we found that the almost thermoneutral $(4+6)$-STIRAP process $R16\rightarrow P12$ can be driven at still slightly higher values of A_0, in the range 0.0033–0.0045

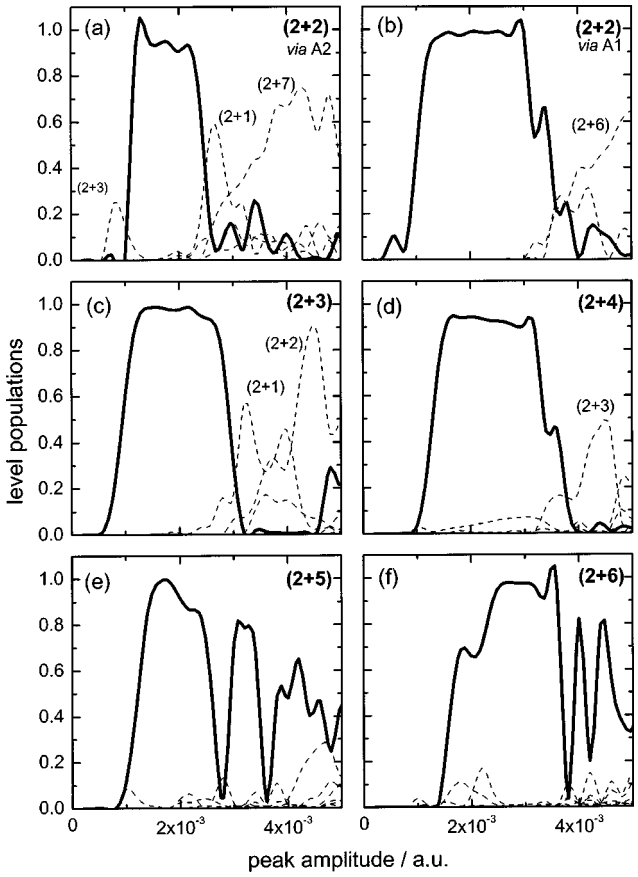

FIG. 5. Field strength dependence of $(2+n)$-STIRAP processes with 80 ps pulses at various fixed $\omega_p-\omega_s$ frequency combinations. The panels show cases giving rise to complete state-specific population transfer as indicated. Full bold lines show the variation of the transfer probability for these nominal transitions. Dashed lines represent competing parallel processes. The $\omega_p-\omega_s$ values in the six panels are (a) 1100–740 cm^{-1}, (b) 1045–695 cm^{-1}, (c) 1075–730 cm^{-1}, (d) 1065–740 cm^{-1}, (e) 1105–765 cm^{-1}, (f) 1095–775 cm^{-1}.

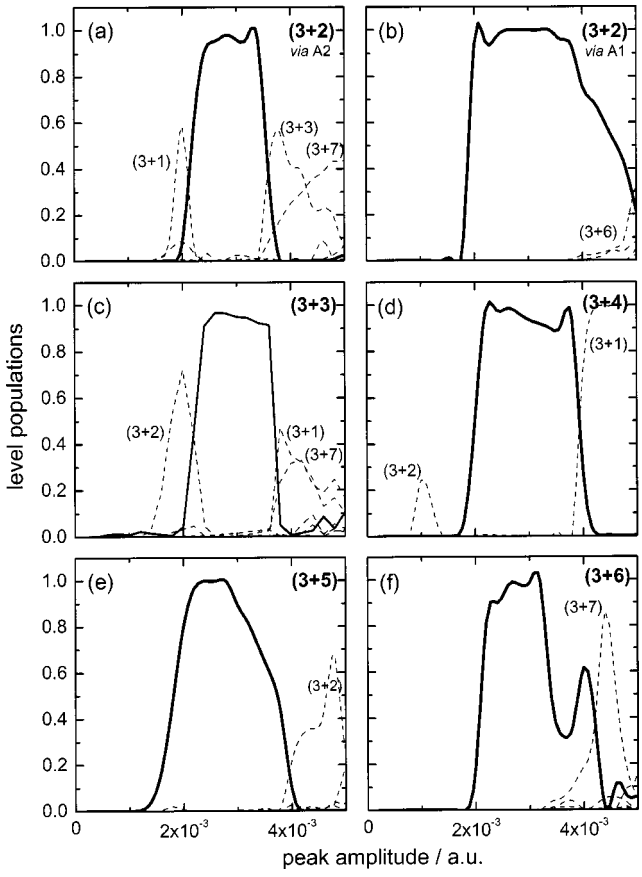

FIG. 6. Field strength dependence of $(3+n)$-STIRAP processes. The $\omega_p-\omega_s$ values in the six panels are (a) 1135–740 cm^{-1}, (b) 1085–690 cm^{-1}, (c) 1135–735 cm^{-1}, (d) 1120–745 cm^{-1}, (e) 1115–755 cm^{-1}, (f) 1145–805 cm^{-1}. All other details are as in Fig. 5.

a.u., when the GPA of the Stokes-pulse becomes large enough to match the adiabaticity condition.

In a qualitative way, the features of robustness following from the analytical analysis of STIRAP (Refs. 8–12, 26) can be redetected in the present results. In particular this concerns the relation between intermediate-level detuning and adiabaticity,[12] which leads to the ''growth'' of the intensity plots with the field strength. As A_0 and hence the GPA, and along with it the adiabaticity parameter are increased, the adiabaticity condition is fulfilled for increasingly higher Δ_1. This qualitative agreement indicates that in some sense MP-STIRAP in a NLS effectively behaves like STIRAP in a TLS.

B. Pulse amplitude

Next we investigate the question how the transfer efficiency for a fixed $\omega_p-\omega_s$-pair varies with the pulse amplitude. In view of the orientational disorder of the molecules in the gas-phase, robustness with respect to the field strength is particularly relevant for gas-phase isomerization, since in any geometrical field-molecule configuration only the projection of the field vector onto the axis is effective. In Figs. 5 and 6 we show the field strength (i.e., A_0) dependence for a number of selected frequency combinations. All these frequency pairs correspond to population maxima for the individual processes as identified in Figs. 3 and 4.

A comparison of the individual panels shows that the interval from about 0.0015 to 0.0045 a.u., corresponding to laser peak intensities of about 80–700 GW cm^{-2}, can be considered a ''characteristic range'' of field strengths for MP-STIRAP in the present system. The low-field threshold of population transfer relates to the breakdown of the adiabatic transfer mechanism due to decreasing GPAs, while at the high field side extensive coupling of the near-degenerate transitions sets in, which destroys the selectivity of population transfer. Irrespective of differences in the details (almost) all transitions have two common features; the rise and fall of the transfer probabilities are very steep, so that for the following discussion to a first approximation the curves can be considered rectangular. The width of these rectangles is roughly as wide as, or wider than the gap from zero amplitude to the rising edge. If the pulse amplitude is adjusted at a value A_0 near the upper edge of the stability range, full transfer occurs over $\approx$50% of the amplitude range from zero to A_0, corresponding, in terms of projection angles, to the range of 0 to about 60°. Hence up to 25% of a randomly oriented sample would be isomerized by such a MP-STIRAP pulse pair.

In principle one should expect to see distinct trends in the A_0-dependence of the transition probabilities connected to the fact that the pulse amplitude is closely linked to the pulse area, the GPA, and the adiabaticity parameter. For example, the thresholds of the curves in Figs. 5 and 6 should reflect the breakdown of the adiabaticity assumption. This low-field threshold behavior, and deviations from it have recently been studied in detail for STIRAP (Ref. 26) and MP-STIRAP (Ref. 22) in simple systems. We should not expect to observe the exponential behavior of adiabatic breakdown[37] in unperturbed form for the present, much more complicated situation. However, the signature of this behavior is still showing up in steep rise of the transfer probabilities. Invoking the adiabaticity criteria in a qualitative way, one should expect the thresholds for the $(3+n)$-processes to be higher than the ones for the $(2+n)$-processes, which is indeed observed. Furthermore, in view of the data in Table II the thresholds within the $(2+n)$-and $(3+n)$-sequences should appear in the order (2-PT, 3-PT)<4-PT<5-PT<6-PT. The examples in Figs. 5 and 6 only partially recover this ordering. The expected trends are obscured mainly due to two reasons. First, the examples shown reflect arbitrary choices for the frequencies. They are not directly comparable with each other, because the values of Δ_1 and Δ_2 are different for the various cases, and the amount of this detuning affects the onset and degree of adiabaticity. Second, the degeneracy-related competition between the Stokes transitions delays some of the thresholds.

We now come back to the detuning of the actual $(m+n)$-photon resonances from their zero-order values. In Figs. 7 and 8 we show the transfer efficiencies for the $(3+n)$-STIRAP processes as functions of A_0 at the zero-order frequencies. It is clear that in most cases MP-STIRAP is not effective on zero-order resonance; indeed for the lower transitions including $(3+1)$ it is not even a good initial guess. It is also clear that such deviations could be expected in view of the dynamical Stark shifts induced by the pulses. On the other hand, the intrinsic robustness of STIRAP with respect to variations in the pulse parameters may mask these shifts. So it remains to be verified if there are other origins for the observed effects. Figure 7 summarizes processes involving pathways through the apex state $A2$. It is seen that for the lower transitions degenerate parallel transitions in some cases proceed at the zero-order resonance frequencies of their competitors. This picture may at first suggest that a strong contribution to the observed resonance defects is related to the near-degeneracies in the system. Yet Fig. 8 makes clear that the shift is also present for the pathways through the apex state $A1$, which are not at all affected by degeneracies or competing parallel processes. Finally we have also verified that the shift is not caused by a possible coupling between the two apex states. In Fig. 8(a) we have included the curve for the on-resonance transfer probability for (3+1)-STIRAP through $A1$ resulting upon the complete removal of the state $A2$ from the basis. Although the presence of $A2$ is seen to have a small effect, there is still no sizable population transfer on zero-order resonance.

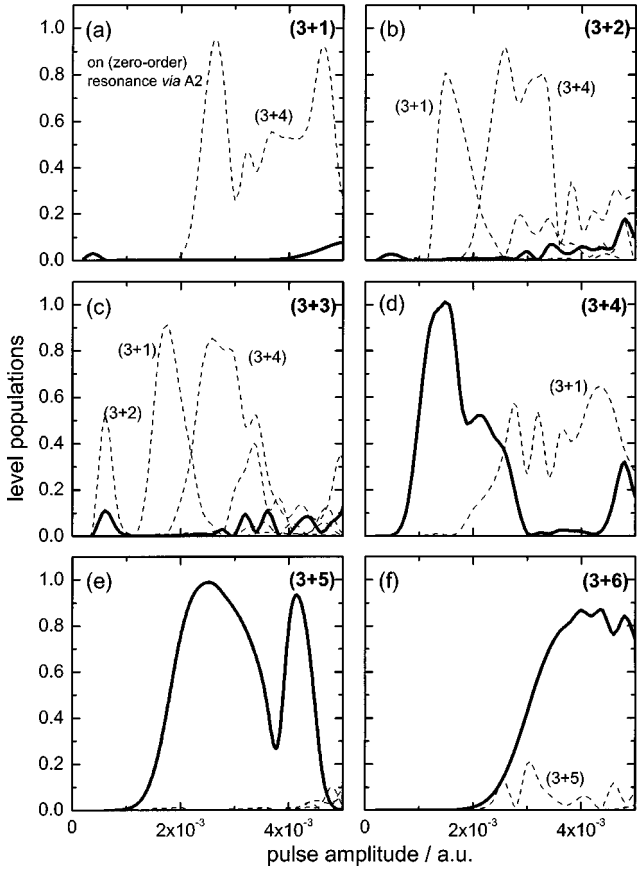

FIG. 7. Field strength dependence of $(3+n)$-STIRAP processes through the apex state $A2$ at the corresponding zero-order resonance frequencies. All other details are as in Fig. 5.

C. Comparison of MP-STIRAP with other techniques

So far we have demonstrated that in the 28-LS modeling the HCN→HNC isomerization MP-STIRAP is feasible and fairly robust, can cope with the difficulties associated with near-degenerate MP-transitions, and can accommodate fairly high photonicities. The straight-forward state specific isomerization to any of the 6 upper target levels contrasts with the results achievable with pump–dump methods using π-pulses or multiple-π-pulses. The close near-degeneracy between the $A2\rightarrow P20$ and $A2\rightarrow P18$ transition frequencies does not allow selective resonant 2-PT and 3-PT through the intermediate level $A2$. Although vibrational wave packet formation is usually associated with fs pulses, these two transitions are strongly coupled even with 80 ps pulses, so that resonant single- and multiple-π-pulses inevitably prepare superposition states. With exactly the same pulse envelopes, by exploiting the intrinsic robustness against variations in Δ_1, the MP-STIRAP method has no problem to drive these transitions selectively.

It now remains to be seen whether MP-STIRAP is competitive with simple (1+1)-STIRAP along overtone sequences.[16] In order to investigate how efficient and robust across-the-barrier multiquantum transitions can be driven with (1+1)-overtone-STIRAP, we have looked at its performance for the two specific processes $R20\rightarrow P16$ and $R18$

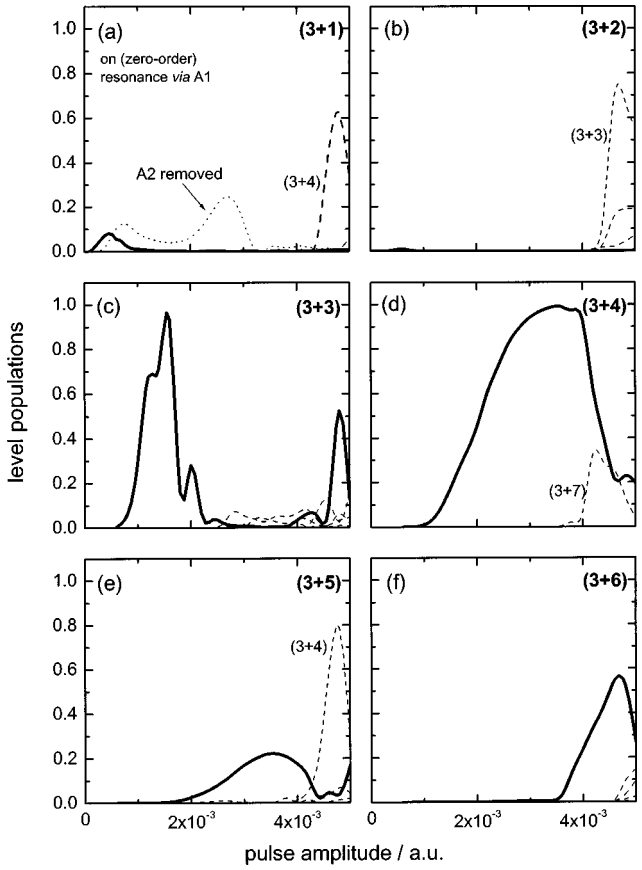

FIG. 8. Field strength dependence of $(3+n)$-STIRAP processes through the apex state $A1$ at the corresponding zero-order resonance frequencies. The dotted line in panel (a) shows the (3+1) population which results upon removal of the state $A2$ from the basis set. All other details are as in Fig. 5.

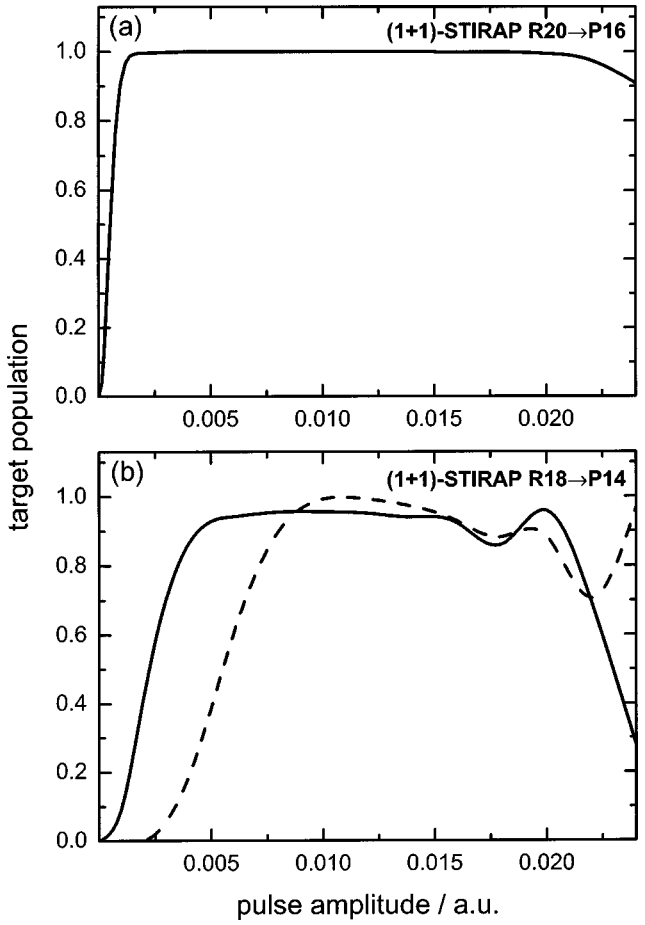

FIG. 9. Field strength dependence of (1+1)-overtone STIRAP processes through the apex state $A2$. (a) The (2+4)-quantum transfer $R20 \rightarrow P16$ at the zero-order resonance frequencies. (b) The (3+5)-quantum transfer R18→P14. The full line is at the zero-order resonance frequencies, the broken line is for a pump detuning of $-2.0\ \mathrm{cm}^{-1}$ and a Stokes detuning of $-1.6\ \mathrm{cm}^{-1}$.

$\rightarrow P14$. These results are to be compared with (2+4)- and (3+5)-STIRAP, respectively.

The data in Table II shows that pulses driving overtone transitions with the same field strength and width as MP-pulses have far smaller GPAs, and this difference is quickly amplified as the number of quanta in the transition increases. Therefore much larger field strengths (or pulse widths) would be required to reach the adiabatic domain. On the other hand, there are no competing and near-degenerate parallel processes, so that the system effectively behaves as a TLS. In this sense it provides perfect conditions for STIRAP, and for adiabatic behavior it requires smaller GPAs than the MP-STIRAP processes.

Indeed both (1+1)-overtone-STIRAP processes can be driven, although with quite different demands on the field strength and with different degrees of robustness. For the (2+4)-quantum transition $P20 \rightarrow R16$, (1+1)-STIRAP is found to have both advantages and disadvantages compared to its MP cousin. It shows a very pronounced stability with respect to variations in the field strength, and even at very high field strengths does not couple to any other transition.

The plot of the transfer efficiencies against pulse amplitude in Fig. 9(a) demonstrates this robustness (note that state-specific transfer proceeds almost up to the Keldysh limit of ionization for molecular systems of ≈ 0.0024 a.u.,[28,38] used as upper end of the plot interval in Fig. 9). However, (1+1)-overtone-STIRAP is far less robust than MP-STIRAP with respect to frequency detuning. At $A_0 = 0.0017$ a.u. there are only two small frequency ranges leading to more than 75% transfer efficiency: an elliptic area centered at the zero-order frequency for transition through $A2$ permitting detunings $\Delta_1 = \pm 1.3\ \mathrm{cm}^{-1}$ and $\Delta_2 \pm 0.5\ \mathrm{cm}^{-1}$, and an even smaller one centered at the zero-order frequency for transition through $A1$. An intensity plot with the scale and resolution of Fig. 3 would appear entirely void.

For the (3+5)-quantum transition $P18 \rightarrow R14$, (1+1)-STIRAP represents no useful alternative to MP-STIRAP at all. As shown in Fig. 9(b) the former requires far too high field strengths, and even at the unlikely peak intensity of $5\ \mathrm{TW\,cm}^{-1}$ ($A_0 = 0.012$ a.u.) the frequencies need to be very precisely tuned in order to obtain complete population transfer. This sensitivity also becomes apparent from the pronounced shifts of the effective field strength thresholds upon weak detuning. In Fig. 9(b) the full-line curve represents the case on zero-order resonance, while the dashed curve with the massively delayed threshold is for a weakly detuned frequency pair (pump detuning $-2.0\ \mathrm{cm}^{-1}$, Stokes detuning $-1.6\ \mathrm{cm}^{-1}$). Contrary to the case on-resonance the latter

eventually leads to ≈100% population transfer. In general, (1+1)-overtone-STIRAP quickly becomes less competitive in comparison with MP-STIRAP as the multiquantum character of the transition driven increases.

D. Additional comments

The $(m+n)$-STIRAP processes investigated above all concern higher-lying levels of our 28-LS, and the lowest states in this basis are often not required for obtaining converged results for these transitions. Indeed we found that the 8 lowest HCN and the 4 lowest HNC states are never appreciably populated in any of the processes at any of the conditions studied in Sec. IV A, and that the bulk of the results can be recovered using a 16-LS obtained from our 28-LS by discarding the 12 states mentioned above. Nevertheless there are cases where it is essential to include the lower states in order to obtain converged results, even if these states fail to become populated at any time. These states then act only through the additional Stark shifts they impose on the system, a mechanism that is most clearly manifest in the deformation of the curves representing the adiabatic instantaneous two-color Floquet states.[29]

Despite using 3D wave functions, our results in effect are for a 1D (bend-coordinate only) model of isomerization. It remains to be seen how they carry over to a full 3D treatment, or termed differently, how the presence of background states would affect the outcome. In the context of STIRAP, this question was first addressed by Coulston and Bergmann,[10] and Rice and co-workers have investigated the problem both for the sequential STIRAP-based control of HCN→HNC isomerization[16] and for an extended 3-pulse STIRAP model.[39,40] In all cases it was concluded that the influence of background states should be weak. On the other hand, it has been shown that background states can significantly modify control fields for the HCN/HNC system.[41,42] Elsewhere the question of background state participation in MP-STIRAP will be considered in detail;[29] we note that the effect varies from being negligible to being dominant.

V. SUMMARY AND CONCLUSIONS

Using a model 28-LS comprising the $J=0$ bend states of the HCN/HNC system, we have shown that isomerization can be achieved with a MP extension of the STIRAP technique. More specifically, we have simulated $(m+n)$-STIRAP transfer, with $m=2$ and 3, and $n=1$ to 6, as well as (4+6)-STIRAP, all proceeding from an excited HCN bend state across the barrier to an excited HNC bend state.

The most notable feature of the 28-LS is the near-degeneracy of several of the Stokes transitions. Nevertheless all the individual competing processes mentioned proceed in a way that is robust with respect to variations in the pulse frequencies and amplitudes. That means that robust and selective population transfer with one pair of counterintuitively ordered pulses is possible even in the presence of pronounced near-degeneracies and overlapping resonances. Previously it has been shown that in a STIRAP setup, the control of branching transitions to exactly degenerate levels requires an additional level and the action of a third pulse.[39] This is not the case in the present situation, which involves competing transitions of *different* photonicities. GPAs, adiabaticity parameters, and resonance detunings for transitions of different photonicities scale differently with field strength, and so it is possible to effectively separate competing individual $(m+n)$-photon processes by simply varying ω and A_0. No modification of the standard STIRAP setup is required, except for the necessity to tune to suitable ranges of pulse amplitudes and frequencies.

In a qualitative and ''overall'' way, the known behavior of STIRAP in TLSs with respect to pulse areas or GPAs and intermediate-level detunings[3,8–12,26] also governs MP-STIRAP. Zero-order resonance frequencies are not usually the right choice. The condition of zero overall detuning provides a first guess, but dynamic Stark shifts resultant from a large number of levels and competition between individual transitions must be taken into account, so that the individual ranges of robust state-specific transfer have to be located more painstakingly, possibly by trial-and-error. Also, the strategy to enforce the approach to the adiabatic regime by increasing the field strength fails if applied in an uncontrolled way. Eventually stronger fields couple the various competing transitions, thus giving rise to the preparation of superposition states.

At face value, our simulations amount to a 1D study of HCN→HNC isomerization. Alternatively the 28-LS, or even more so the related 16-LS described in Sec. IV D, can be viewed as models for the study of population transfer in many-level extended Λ-systems, which incorporate essential properties of realistic molecular system. They differ from usual minimal models, which they augment, in several respects, namely the extension of the Λ-system in all directions, the doubling of the apex state, and the presence of distortions in the anharmonic progressions giving rise to overlapping resonances of different photonicities. All these properties are likely to also be features of realistic molecular systems beyond the special case of the HCN/HNC system. The 16-LS represents a minimal model system with such realistic features.

Summing up, we have verified by numerical simulations that in a NLS of moderate complexity modeling molecular isomerization, MP-STIRAP is a suitable method for obtaining robust and efficient state-to-state population transfer across a barrier, even in case of the presence of competing, near-degenerate transitions. Extended stretches of vibrational progressions can be traversed in a single step. It should be possible to implement a few-step sequential MP-STIRAP based control scheme of isomerization reactions in analogy to the STIRAP-based method of Kurkal and Rice.[17]

ACKNOWLEDGMENT

This work was sponsored by the Austrian Science Fund within the framework of the Special Research Program F016 ''ADLIS.''

[1] S. A. Rice, and M. Zhao, *Optical Control of Molecular Dynamics* (Wiley, New York, 2000).
[2] M. Dohle, J. Manz, G. K. Paramonov, and H. Quast, Chem. Phys. **197**, 91 (1995).

[3] B. W. Shore, K. Bergmann, A. Kuhn, S. Schiemann, J. Oreg, and J. H. Eberly, Phys. Rev. A **45**, 5297 (1992).
[4] J. Allen and J. H. Eberly, *Optical Resonance and Two-Level Atoms* (Wiley, New York, 1975).
[5] R. S. Judson and H. Rabitz, Phys. Rev. Lett. **68**, 1500 (1992); W. Zhu and H. Rabitz, J. Chem. Phys. **109**, 385 (1998); J. M. Geremia, W. Zhu, and H. Rabitz, *ibid.* **113**, 10841 (2000).
[6] A. Assion, T. Baumert, T. Bergt, B. Brixner, B. Kiefer, M. Seyfried, M. Strehle, and G. Gerber, Science **282**, 919 (1998); T. Brixner, B. Kiefer, and G. Gerber, Chem. Phys. **267**, 241 (2001).
[7] T. Feurer, A. Glaß, T. Rozgonyi, R. Sauerbrey, and G. Szabo, Chem. Phys. **267**, 223 (2001); C. Daniel, J. Full, L. Gonzalez *et al.*, *ibid.* **267**, 247 (2001).
[8] J. Oreg, F. T. Hioe, and J. H. Eberly, Phys. Rev. A **29**, 690 (1984); J. Oreg, G. Hazak, and J. H. Eberly, *ibid.* **32**, 2776 (1985); J. R. Kuklinski, U. Gaubatz, F. T. Hioe, and K. Bergmann, *ibid.* **40**, 6741 (1989); C. E. Carroll and F. T. Hioe, *ibid.* **42**, 1522 (1990).
[9] U. Gaubatz, P. Rudecki, S. Schiemann, and K. Bergmann, J. Chem. Phys. **92**, 5363 (1990); H.-G. Rubahn, E. Konz, S. Schiemann, and K. Bergmann, Z. Phys. D: At., Mol. Clusters **22**, 401 (1991).
[10] G. W. Coulston and K. Bergmann, J. Chem. Phys. **96**, 3467 (1992).
[11] K. Bergmann, H. Theuer, and B. W. Shore, Rev. Mod. Phys. **70**, 1003 (1998).
[12] N. V. Vitanov and S. Stenholm, Phys. Rev. A **55**, 648 (1997); N. V. Vitanov and S. Stenholm, Opt. Commun. **135**, 394 (1997).
[13] Y. Ohta, T. Yoshimoto, and K. Nishikawa, Chem. Phys. Lett. **316**, 551 (2000).
[14] J. E. Combariza, B. Just, J. Manz, and G. K. Paramonov, J. Phys. Chem. **95**, 10351 (1991); J. E. Combariza, S. Görtler, B. Just, and J. Manz, Chem. Phys. Lett. **195**, 393 (1992); M. V. Korolkov, J. Manz, and G. K. Paramonov, J. Chem. Phys. **105**, 10874 (1996).
[15] W. Jakubetz and B.-L. Lan, Chem. Phys. **217**, 375 (1997).
[16] V. Kurkal and S. A. Rice, Chem. Phys. Lett. **344**, 125 (2001).
[17] Y. B. Band and P. S. Julienne, J. Chem. Phys. **95**, 5681 (1991).
[18] J. Oreg, K. Bergmann, B. W. Shore, and S. Rosenwaks, Phys. Rev. A **45**, 4888 (1992).
[19] B. W. Shore, K. Bergmann, J. Oreg, and S. Rosenwaks, Phys. Rev. A **44**, 7442 (1991).
[20] V. S. Malinovsky and D. J. Tannor, Phys. Rev. A **56**, 4929 (1997).
[21] S. Guérin and H. R. Jauslin, Eur. Phys. J. D **2**, 99 (1998); S. Guérin, L. P. Yatsenko, and H. R. Jauslin, Phys. Rev. A **63**, 031403 (2001).
[22] K. Drese and M. Holthaus, Eur. Phys. J. D **5**, 119 (1999).
[23] L. P. Yatsenko, S. Guérin, T. Halfmann, K. Böhmer, B. W. Shore, and K. Bergmann, Phys. Rev. A **58**, 4683 (1998); S. Guérin, L. P. Yatsenko, T. Halfmann, B. W. Shore, and K. Bergmann, *ibid.* **58**, 4691 (1998); K. Böhmer, T. Halfmann, L. P. Yatsenko, B. W. Shore, and K. Bergmann, *ibid.* **64**, 023404 (2001).
[24] For experimental applications, see N. Dam, S. Stolte, and J. Reuss, Chem. Phys. **135**, 437 (1989); **140**, 217 (1990); J. Oomens, L. Oudejans, J. Reuss, and A. Fayt, *ibid.* **187**, 57 (1994).
[25] T. S. Ho and S. I. Chu, J. Phys. B **17**, 2101 (1984).
[26] T. A. Laine and S. Stenholm, Phys. Rev. A **53**, 2501 (1996); N. V. Vitanov and S. Stenholm, Opt. Commun. **127**, 215 (1996).
[27] M. Holthaus and B. Just, Phys. Rev. A **49**, 1950 (1994).
[28] S. Chelkowski, A. D. Bandrauk, and P. B. Corkum, Phys. Rev. Lett. **65**, 2355 (1990).
[29] I. Vrábel and W. Jakubetz (unpublished).
[30] W. Jakubetz, Faraday Discuss. **113**, 355 (1999).
[31] J. M. Bowman, B. Gazdy, J. A. Bentley, T. J. Lee, and C. E. Dateo, J. Chem. Phys. **99**, 308 (1993).
[32] W. Jakubetz, E. Kades, and J. Manz, J. Phys. Chem. **97**, 12609 (1993).
[33] I. Vrábel and W. Jakubetz (unpublished).
[34] A. Peirce, M. Dahleh, and H. Rabitz, Phys. Rev. A **37**, 4950 (1988); S. Shi and H. Rabitz, J. Chem. Phys. **92**, 2927 (1990).
[35] W. Jakubetz, J. Manz, and H.-J. Schreier, Chem. Phys. Lett. **165**, 100 (1990).
[36] F. Bloch and A. Siegert, Phys. Rev. **57**, 522 (1940); D. R. Dion and J. O. Hirschfelder, Adv. Chem. Phys. **35**, 265 (1976).
[37] J. P. Davis and P. Pechukas, J. Chem. Phys. **64**, 3129 (1976).
[38] P. Dietrich and P. B. Corkum, J. Chem. Phys. **97**, 3187 (1992).
[39] M. N. Kobrak and S. A. Rice, Phys. Rev. A **57**, 2885 (1998).
[40] V. Kurkal and S. A. Rice, J. Phys. Chem. B **105**, 6488 (2001).
[41] S. P. Shah and S. A. Rice, J. Chem. Phys. **113**, 6536 (2000).
[42] W. Jakubetz and B.-L. Lan, J. Chem. Phys. **117**, 7968 (2002).